Magnetism and magnetization dynamics in thin film ferromagnets

Verhagen, T.G.A.

CHAPTER 6

Spin-orbit torque in SiO_X/Co/Cu bilayers

Traditional spintronic devices consist of two ferromagnetic layers, the polarizer and the free layer, with a normal nonmagnetic spacer, a tunnel barrier or a domain wall in between and either in a perpendicular or lateral geometry with respect to the current. Basically, the current flowing through the first ferromagnetic layer becomes polarized and can change the magnetization direction of the second ferromagnetic layer via the spin transfer torque mechanism.

Recently, experiments and theory have shown that there are alternative mechanisms that can produce a spin torque, based on the spin-orbit interaction (SOI). The SOI transfers orbital angular momentum from the lattice to the spin system. Up to now, the spin Hall and Rashba effects, both based on the SOI, are used to exploit the coupling between the electron spin and the orbital motion. The spin-orbit torque (SOT) in ferromagnetic structures, generated by such SOIs, received a lot of attention as it shows to be an efficient electric magnetization switch mechanism that only needs one ferromagnetic layer.

Spin-orbit torques can be related to inversion symmetry either in the bulk of a material or in thin film structures, resulting in a Rashba or a Dresselhaus spin-orbit coupling, respectively. Well known systems where such a lack of bulk inversion symmetry can be found are semiconductors with the zinc blende structure such as (Ga,Mn)As [49–51] or crystals from the B20 space group such as FeGe [52] and MnSi [53]

which show a chiral spin-orbit interaction, described by the rotationally invariant Dzyaloshinsky-Moriya (DM) interaction. In these systems, as a consequence, non-trivial spin structures can occur.

The broken inversion symmetry in these structures gives rise to a static electric field $\mathbf{E}$ in the laboratory frame at rest, that in turn gives rise to a magnetic field $\mathbf{B}$ in the reference frame of an object moving with momentum $\hbar\mathbf{k}$. Recently, experiments and theory indicated that also in ultrathin metallic multilayers with a built-in lack of inversion symmetry, Rashba spin-orbit coupling might be present. A static electric field $\mathbf{E} = E_0 e_z$ in the laboratory rest frame, where e_z points normal to the surface of the multilayers, produces a magnetic field $\mathbf{B} \propto k_x e_y - k_y e_x$ in the frame of the moving object, where $k_x e_y - k_y e_x$ is known as the Rashba spin-orbit coupling.

Up to now, the ferromagnetic layer has either been asymmetrically sandwiched between a heavy metal layer and an oxide layer, e.g. Pt/ Co/AlO_x or Ta/CoFeB/MgO [14, 54–57] or in periodic crystals that lack inversion symmetry like (Ga,Mn)As [49–51].

Two different torques are found in these experiments; one torque is an even function of the unit vector of magnetization direction $\boldsymbol{m}$ and the other torque is an odd function of $\boldsymbol{m}$. Up to the lowest order, the even torque $\boldsymbol{T}^{\parallel} = \mathrm{T}^{\parallel}\boldsymbol{m} \times [(\hat{\boldsymbol{e}}_z \times \boldsymbol{E}) \times \boldsymbol{m}]$, where $\boldsymbol{E}$ is the applied electric field and $\hat{\boldsymbol{e}}$ is a unit vector perpendicular to the interface of the ferromagnetic heterostructure, is expected to be driven by the spin current due to the spin Hall effect (SHE) in the heavy-metal layer. The torque has the same shape as the damping term in the Landau-Lifschitz-Gilbert equation and is then also called damping-like torque. The odd torque $\boldsymbol{T}^{\perp} = \mathrm{T}^{\perp}(\hat{\boldsymbol{e}}_z \times \boldsymbol{E}) \times \boldsymbol{m}$ is expected to originate from the effective magnetic field due to spin dependent scattering in combination with the Rashba interaction, which originates from the broken inversion symmetry in the ferromagnetic heterostructures. This torque has the same shape as the field term in the Landau-Lifschitz-Gilbert equation and is then also called field-like torque.

However, there are theoretical predictions that the SHE can also be induced into a light normal metal like Cu or Al, when it is sandwiched between two different oxide layers or insulators [66], due to interfacial spin-orbit coupling. In this Chapter, we use ferromagnetic resonance and Hall measurements to show that also in an ultrathin Co layer sandwiched between SiO_x and Cu more damping is present than would be expected from the Cu layer, which only has weak bulk spin-orbit coupling. We attribute this to the Rashba spin-orbit torque induced by to the broken inversion symmetry. We investigate this in a way similar to

Chapter 5, by comparing SiO_x/Co(d)/Cu bilayers with Cu/Co(d)/Cu trilayers.

6.1 Experiment

The following films were grown: Co(d)/Pt(10), Pt(10)/Co(d)/Pt(10), Co(d)/Cu(10) and Cu(10)/Co(d)/Cu(10). The numbers in parentheses represent the layer thickness in nanometers. They were deposited on naturally oxidized Si(100) in a UHV chamber (base pressure $1 \cdot 10^{-9}$ mbar) using DC magnetron sputter deposition with argon as plasma at room temperature from 3N5 Co, 3N5 Cu and 3N5 Pt targets. To take into account both interfaces of the Co layer, we call the Co/Pt and Co/Cu bilayers in this Chapter SiO_x/Co/Cu and SiO_x/Co/Pt. Also, since the thicknesses of the Cu- and Pt-layers are not going to be varied, we call them Co(d)/Pt etc. The deposition rate was measured by X-ray reflectivity (XRR) using Cu-Kα radiation and was 0.58 Å/s for Co, 1.90 Å/s for Cu and 1.54 Å/s for Pt respectively. Magnetization measurements were performed using the reciprocating sample option (RSO) in a SQUID-based magnetometer (MPMS XL-7 from Quantum Design). Ferromagnetic resonance (FMR) was measured using a Bruker EMX-plus X-band spectrometer in a TE_{011} cavity with 100 kHz modulation frequency and 1 G modulation amplitude with a maximum DC-field of 0.65 T. The sample was fixed on a Rexolite 1422 rod and a goniometer was used to vary the angle. For electrical characterization, the samples were patterned into Hall bar structures, 50×1000 μm^2, using negative resist, electron beam lithography and ion beam etching. Resistivity measurements were performed at room temperature using the lock-in technique, with a variable ac-current modulated at 1106 Hz.

6.2 Results

Figure 6.1.a shows the angular dependent peak-to-peak linewidth H_{pp} of the SiO_x/Co(2.6)/Pt, Pt/Co(2.6)/Pt, SiO_x/Co(2.6)/Cu and Cu/Co(2.6)/Cu multilayers. Clearly visible is that ΔH_{pp} of the Cu/Co/Cu trilayer is much smaller than ΔH_{pp} of the Pt/Co/Pt and SiO_x/Co/Pt films, but also much smaller than ΔH_{pp} of the SiO_x/Co/Cu bilayer. In Figure 6.1.b, the angular dependent resonant fields H_r are plotted. H_r of the Pt/Co/Pt trilayer is larger than H_r of the other multilayers, for which H_r is almost the same.

In Figure 6.2, we take a closer look to the magnetic properties of the multilayers. The effective demagnetization fields $4\pi M_{eff}$, obtained from

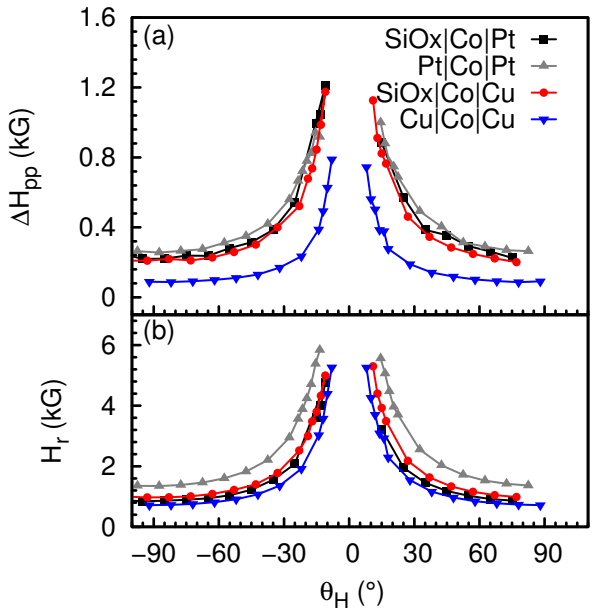

Figure 6.1: Angular dependence of the peak-to-peak linewidth $H_{\rm pp}$ (a) and the resonance field H_r (b) as a function of the applied field direction θ_H for a SiO_x/Co(2.6)/Pt (black ■), SiO_x/Co(2.6)/Cu (red ●), Cu/Co(2.6)/Cu (blue ▼) and Pt/Co(2.6)/Pt (green ▲) multilayers.

the analysis of the angular dependent FMR (see Chapter 5), and the saturation magnetization $4\pi M_s$, obtained using a magnetometer, are plotted as a function of the Co thickness d. The data for the Pt/Co(1.7)/Pt trilayer is not included in the analysis, as two resonance modes [152] are observed in this sample and the origin of this mode is not clear.

For large Co thicknesses, $4\pi M_s$ reaches the saturation magnetization value of bulk Co in all samples, as indicated by the horizontal dotted line. In the Pt/Co/Pt and SiO_x/Co/Pt samples, $4\pi M_s$ reaches the bulk saturation magnetization value also for small Co thicknesses. However, in the Cu/Co/Cu and SiO_x/Co/Cu samples, $4\pi M_s$ becomes gradually smaller for thinner Co layers. For all samples, $4\pi M_{\rm eff}$ is lower than $4\pi M_s$ of bulk Co. For the Pt/Co/Pt and SiO_x/Co/Pt samples, $4\pi M_{\rm eff}$ decreases rapidly with a decreasing Co thickness. $4\pi M_{\rm eff}$ decreases also for Cu/Co/Cu samples, but the change is much less than

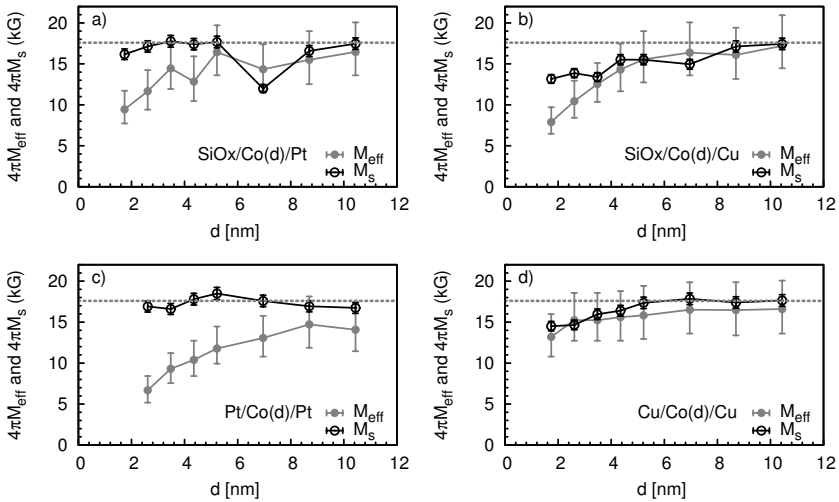

Figure 6.2: The effective demagnetization $4\pi M_{\text{eff}}$ (closed symbols) and the saturation magnetization $4\pi M_s$ (open symbols), as a function of the thickness d of the Co layer in (a) the SiO_x/Co/Pt bilayers; in (b) the SiO_x/Co/Cu bilayers, in (c) the Pt/Co(d)/Pt trilayers and in (d) the Cu/Co/Cu (d) trilayers. $4\pi M_{\text{eff}}$ is the average value of 10 simulations with a g-factor between 1.8 and 2.2 [152] and the maximum and minimum value from this simulations. The dashed line indicates saturation magnetization of bulk Co.

for the SiO_x/Co/Pt and Pt/Co/Pt multilayers. The SiO_x/Co/Cu bilayers show a strong decrease in $4\pi M_{\text{eff}}$.

To compare $4\pi M_{\text{eff}}$ between the different multilayers, this quantity is plotted in Figure 6.3.a for the Cu/Co(d)/Cu and Pt/Co(d)/Pt trilayers and in Figure 6.4.a for the SiO_x/Co(d)/Pt and a SiO_x/Co(d)/Cu bilayers. Clearly visible is that $4\pi M_{\text{eff}}$ for both bilayers grown on SiO_x shows almost the same behavior. For thick Co layers, $4\pi M_{\text{eff}}$ is lower than M_s of bulk Co. When decreasing the Co thickness d, $4\pi M_{\text{eff}}$ becomes smaller for both the SiO_x/Co/Cu and SiO_x/Co/Pt bilayers and both bilayers follow the same trend.

In Figure 6.3.b, the Gilbert damping α is plotted for the Cu/Co(d)/Cu and Pt/Co(d)/Pt trilayers and in Figure 6.4.b for for the SiO_x/Co(d)/Pt and a SiO_x/Co(d)/Cu bilayers. α in the Pt/Co/Pt trilayer increases rapidly, as Pt is a good spin sink. For the Cu/Co/Cu trilayer, α is almost constant up to the lowest Co thickness, as Cu is a bad spin sink.

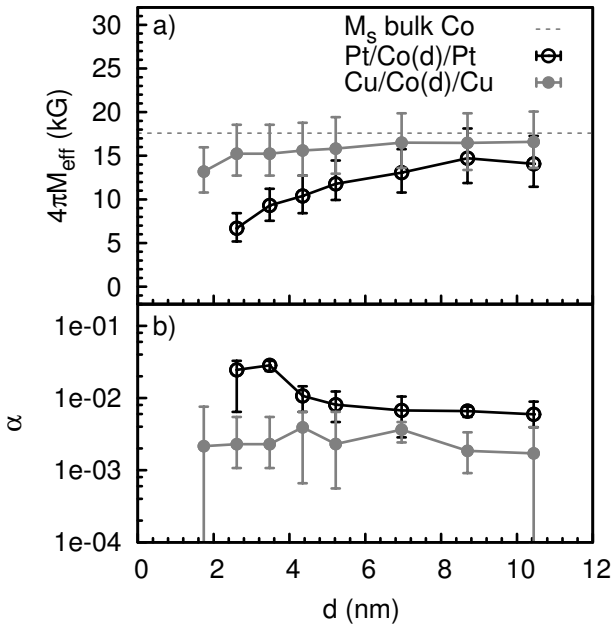

Figure 6.3: The effective demagnetization $4\pi M_{\text{eff}}$ (a) and the damping α (b), as a function of the thickness d of the Co layer in the Pt/Co(d)/Pt (black ○) and Cu/Co(d)/Cu (gray ●) trilayers. Shown are the average values of 10 simulations with a g-factor between 1.8 and 2.2 [152] and the maximum and minimum value from this simulations.

The SiO_x/Co/Pt bilayer shows also a rapid increase in α. However, although Cu is a bad spin sink, α of the SiO_x/Co/Cu bilayer behaves *the same* as the SiO_x/Co/Pt bilayer in contrast to what was seen in the trilayers.

Figure 6.5 shows the thickness dependence of the spatial variations in the direction of the easy axis $\Delta(\theta_H)$ (a) and demagnetization field $\Delta(4\pi M_{\text{eff}})$ (b) for the four multilayers, as obtained from analysis of the angular dependence of the FMR. For decreasing Co thicknesses, both $\Delta(\theta_H)$ and $\Delta(4\pi M_{\text{eff}})$ increase for all sets of multilayers.

In Figure 6.6.a, the perpendicular anisotropy field $H_\perp = 4\pi M_s - 4\pi M_{\text{eff}}$, where $H_\perp = 2K_\perp/M_s$, is plotted as a function of the inverse thickness of the Co layer. Clearly visible is that for all samples $H_\perp$ is present. $H_\perp$ is largest in the Pt/Co/Pt trilayer, followed by the SiO_x/Co/Pt and SiO_x/Co/Cu bilayers respectively while $H_\perp$ of the Cu/Co/

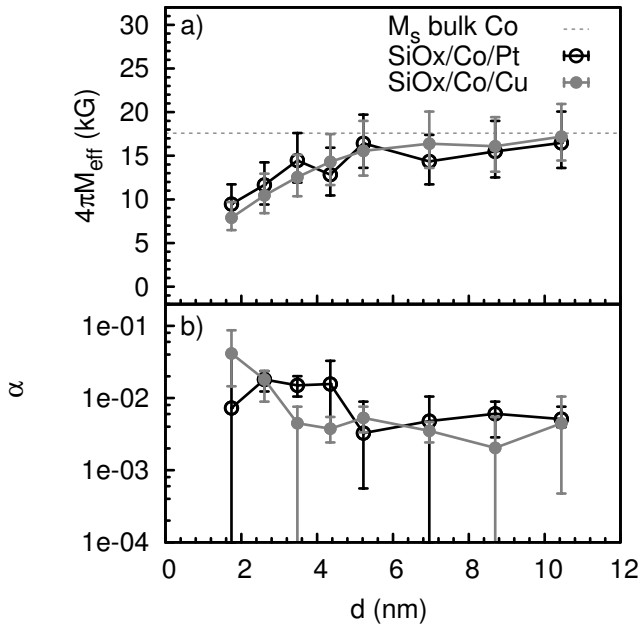

Figure 6.4: The effective demagnetization $4\pi M_{\text{eff}}$ (a) and the damping α (b), as a function of the thickness d of the Co layer in the SiO_x/Co(d)/Pt (black ○) and SiO_x/Co(d)/Cu (gray ●) bilayers. Shown are the average values of 10 simulations with different g-factor and the maximum and minimum value from this simulations.

Cu trilayer is very small. $K_\perp$ consists of a contribution of the anisotropy of the interface atoms K_s and the inner atoms of the magnetic layer K_v with thickness d

$$K_\perp = K_v + 2\frac{K_s}{d}. \tag{6.1}$$

In Figure 6.6.b, $K_\perp d$ is plotted as a function of the inverse thickness of the Co layer. $K_\perp$ does not show a linear relation, as would be expected following equation 6.1. For larger Co thicknesses, $K_\perp d$ is largest for the Pt/Co/Pt trilayer. When decreasing the Co thickness, $K_\perp d$ increases for the Pt/Co/Pt trilayer, but decreases for the Cu/Co/Cu and SiO_x/Co/Cu multilayers and varies for the SiO_x/Co/Pt bilayer. For the thinnest Co layer, $K_\perp d$ is almost the same for the SiO_x/Co/Cu, SiO_x/Co/Pt and Pt/Co/Pt multilayers.

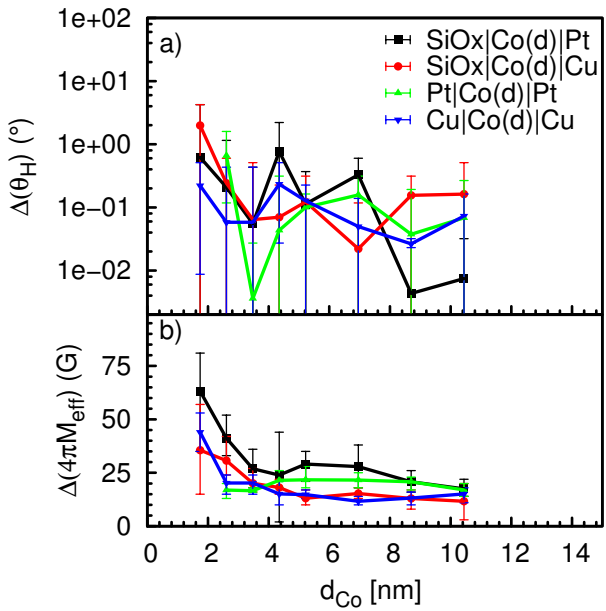

Figure 6.5: The spatial variations in the direction of the easy axis, $\Delta(\theta_H)$ (a) and the effective demagnetization field, $\Delta(4\pi M_{eff})$ (b), as a function of the thickness d of the Co layer in the $SiO_x/Co(d)/Pt$ (black ■), $SiO_x/Co(d)/Cu$ (red ●), $Cu/Co(d)/Cu$ (blue ▼) and $Pt/Co(d)/Pt$ (green ▲) multilayers. Shown are the average values of 10 simulations with different g-factor and the maximum and minimum value from this simulations.

6.3 δ-doping with magnetic impurities

A possible explanation for the increased damping in the $SiO_x/Co/Cu$ bilayers is the presence of magnetic impurities in the Cu layer. In deposition systems where magnetic materials are deposited, there is always a chance that other materials slowly become contaminated with the magnetic impurities. Adding magnetic impurities to a normal metal [22] or a superconductor [166] can dramatically change the properties of these materials. Furthermore, Niimi et al. showed that the spin Hall angle increases when Ir [63] and Bi [64] impurities are added to Cu.

To study the influence of magnetic impurities on the damping of the ferromagnetic layer, we used the δ-doping technique as used before

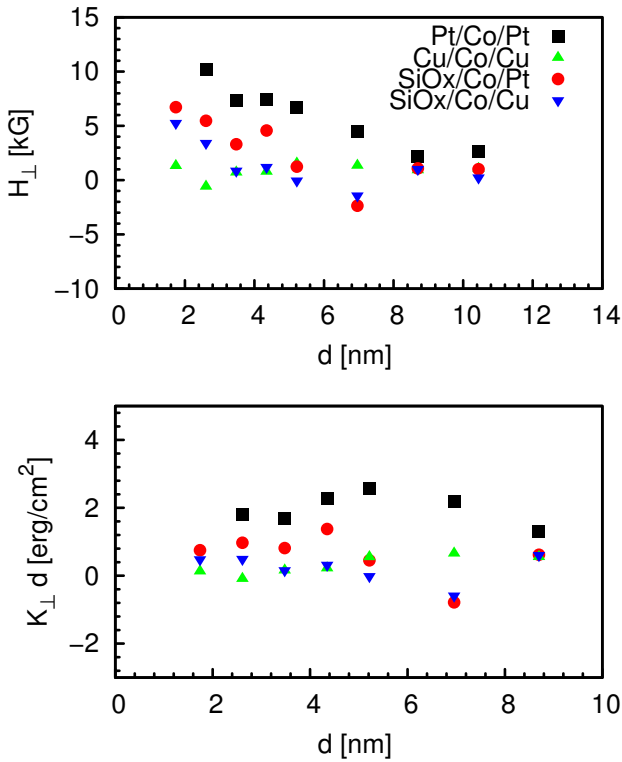

Figure 6.6: The perpendicular anisotropy field $H_\perp$ (a) as a function of the Co thickness d and $K_\perp d$ (b) and as a function of the inverse thickness of the Co layer for the Pt/Co(d)/Pt (black ■), SiO_x/Co(d)/Pt (red ●), SiO_x/Co(d)/Cu (blue ▼) and Cu/Co(d)/Cu (green ▲) multilayers.

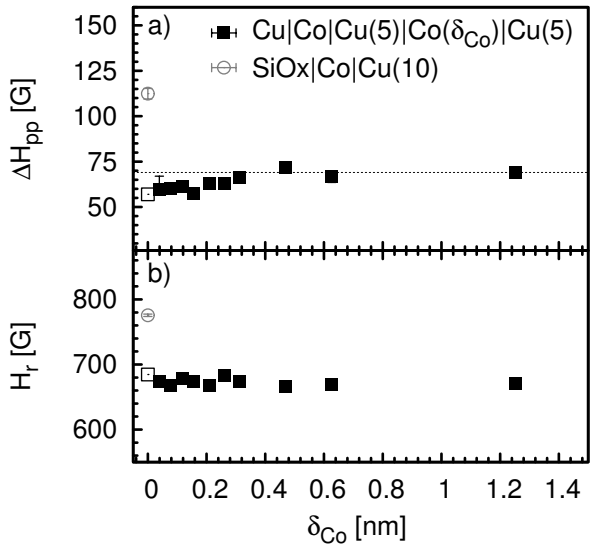

Figure 6.7: Peak-to-peak linewidth ΔH_{pp} (a) and resonance field H_r (b) for Cu/Co(3.6)/Cu(5)Co(δ_{Co})/Cu(5) multilayer as a function of the thickness of the Co impurity layer δ_{Co} (black ■, with the point $\delta_{\mathrm{Co}} = 0$ indicated with a black □). As a reference, also ΔH_{pp} and H_r of a SiO_x/Co(3.6)/Cu bilayer are plotted (gray ○). As a guide for the eye, the grey dotted line indicates the maximum ΔH_{pp}.

by Marrows and Hickey [167] to investigate the role of impurities in GMR systems. With the δ-doping technique, a very thin magnetic layer is added to the multilayer. To study the effect of Co impurities on the SiO_x/Co/Cu bilayer, we grew Cu/Co(3.6)/Cu(5)/Co(δ_{Co})/Cu(5) multilayers where the thickness of the δ_{Co} impurity layer is varied between 0 and 1.2 nm. For the growth of this very thin Co layers, a Co deposition rate of 0.13 Å/s was used.

Figure 6.7.a shows ΔH_{pp} of Cu/Co(3.6)/Cu(5)/Co(δ_{Co})/Cu(5) multilayers as a function of the Co impurity layer δ_{Co}. Clearly visible is that ΔH_{pp} increases as the thickness of the impurity layer increases and saturates already for a 0.32 nm thick impurity layer. In Figure 6.7.b, H_r of these samples is shown. H_r is almost constant for the whole impurity layer thickness range, which shows that the thickness of the 3.6 nm thick Co layer does not vary from sample to sample and the Co impurity layer does not couple to the thick Co layer. As a refer-

ence, in Figure 6.7 also ΔH_{pp} and H_r of the SiO_x/Co(3.6)/Cu bilayer are shown. Clearly visible is that both values are much larger than for the Cu/Co(3.6)/Cu(5)Co(δ_{Co})/Cu(5) multilayers, which indicates that magnetic impurities do not cause the large increase of the damping in SiO_x/Co/Cu bilayers.

6.4 Evaluation of the FMR measurements

The main point to be discussed is the observation of an unexpectedly large increase in the Gilbert damping and the resonance field in SiO_x/Co(d)/Cu bilayers with small Co thickness. This is unexpected in the sense that the Cu layer, which is supposed to be a bad spin sink, is not supposed to generate a spin pumping effect as seen by the FMR line broadening.

This is emphasized by the fact that the trilayers Cu/Co(d)/Cu and Pt/Co(d)/Pt show the difference expected for the good spin sink Pt and the bad spin sink Cu. The angular dependence of ΔH_{pp} and H_r (Figure 6.1) and the extracted values for the damping parameter α (Figure 6.3) show α to be independent of d in the case of Cu, and increasing with decreasing d in the case of Pt, with more than an order of magnitude difference at the lowest thicknesses. Other parameters of the trilayer also behave in an understandable way. As shown in Figure 6.3.a, $4\pi M_{\mathrm{eff}}$ of the Pt/Co(d)/Pt trilayer decreases with decreasing d, due to the increasing perpendicular magnetic anisotropy (PMA). For the Cu case the decrease is smaller, as expected of the lower PMA of the Co/Cu interface.

For both types of trilayers, $\Delta(\theta_H)$ and $\Delta(4\pi M_{\mathrm{eff}})$ becomes larger for very thin Co films. This is expected for very thin Co layers, as the roughness of the Cu and Pt buffer layer introduces $\Delta(\theta_H)$ and $\Delta(4\pi M_{\mathrm{eff}})$ of the Co film and the exchange coupling is not strong enough to average out these variations [153]. Although for thicker Co films the roughness of the Cu and Pt buffer layer does not change, all magnetic moments in the Co film become parallel to the film plane. Furthermore, the spatial variation in both sets of trilayers shows the same order of variation as the data set of Mizukami et al. [153], that were used to derive the spin pumping theory [67].

In contrast, the behavior of the SiO_x/Co/Cu and SiO_x/Co/Pt bilayers does not show the expected behavior. The angular dependence of ΔH_{pp} and H_r (Figure 6.1) and the extracted values for the damping parameter α (Figure 6.4) show α to be increasing with decreasing d in the case of both Cu and Pt.

Other parameters of the bilayer also do not behave in an understandable way. As shown in Figure 6.4.a, $4\pi M_{\text{eff}}$ of the SiO_x/Co(d)/Pt and SiO_x/Co(d)/Cu bilayers both decrease with decreasing d. The increase of the PMA for very thin Co thicknesses in the SiO_x/Co/Cu bilayer is unexpected, as the influence of the interfacial anisotropy of the SiO_x/Co interface is negligible since K_s for a SiO_2/Co interface is of the same order as for a Co/Cu interface [168]. This shows that the huge increase in M_{eff} is probably not due to the PMA.

For both types of bilayers, $\Delta(\theta_H)$ and $\Delta(4\pi M_{\text{eff}})$ becomes larger for very thin Co films. The spatial variation in both sets of bilayers shows the same order of variation as the data set of the trilayers. Furthermore, the spin sink ability of the Cu can in principle be modified by adding magnetic impurities. But, the influence of magnetic impurities on the change in ΔH_{pp} is only small, as can be seen in Figure 6.7.

The observed behaviour is not easy to explain using different magnetic anisotropies or growth related issues. The measurements suggest that there is an extra intrinsic damping mechanisms present in the bilayers. A possible candidate to furnish such a mechanism is the effect of the lack of inversion symmetry, which could give rise to Rashba- or spin Hall-like torques. From the FMR spectra, already a first estimate can be made of extra torques acting on the system. When we compare the SiO_x/Co/Cu and Cu/Co/Cu samples, and assume that the extra damping present in the SiO_x/Co/Cu bilayers is only due to the lack of inversion symmetry, H_r and H_{pp} are 262 and 113 G larger in the SiO_x/Co(2.6)/Cu bilayer than in the Cu/Co(2.6)/Cu trilayer. This indicates a field-like torque component of approximately 262 G while the spin transfer-like torque is approximately 113 G. This corresponds well with the size of the torques found very recently by Hall effect measurements in AlO_x(2)/Co(0.6)/Pt(3) trilayers [169].

In the next section, we look at the influence of the spin Hall effect on the FMR spectra, by sending a current through the Pt layer in a Co/Pt bilayer.

Furthermore, we will have a closer look at the possible existence of this Rashba spin-orbit torque. In particular, we look at the influence of the substrate and especially its dielectric properties. In the case of oxide interfaces involving $SrTiO_3$, which has a very high dielectric constant, it has been shown that the Rashba spin-orbit interaction can even be tuned with an electric field [170].

These extra torques can be also characterized using Hall measurements. We performed a first set of measurements of the Hall coefficients of a SiO_x/Co(2.6)/Cu bilayer and a Cu/Co(2.6)/Cu trilayer. Although the results give indications for the existence of extra torques, they are

not yet unequivocal and will be discussed in Appendix A.

6.5 Electric manipulation of the magnetization precession using the SHE

In Chapter 5, the spin current injected in the Pt layer was converted to an electric current using the inverse spin Hall effect. Ando et al. [58] showed that the reciprocal process is also possible. When a current is sent through the Pt layer, a spin current is generated via the spin Hall effect. This spin current J_s can manipulate the magnetization precession, which can be described as an extra torque $\boldsymbol{\tau}$

$$\boldsymbol{\tau} = -\frac{\gamma J_s}{M_s A d}\boldsymbol{m} \times (\boldsymbol{m} \times \boldsymbol{\sigma}) \tag{6.2}$$

in the Landau-Lifshitz-Gilbert equation [58]. In this section, we want to know how much the spectrum of a SiO_x/Co/Pt bilayer changes when a spin current is injected.

In Figure 6.8.a, the FMR spectra of a SiO_x/Co(5)/Pt bilayer are shown where the magnetization relaxation is manipulated using the SHE. Using the same geometry used to measure V_{ISH}, see Figure 5.8, now a dc current is sent through the SiO_x/Co(5)/Pt bilayer. The absorption derivative I is normalized by dividing the measured values by the maximum absorption derivative when no current is applied. When a current is sent through the bilayer, H_r increases. Furthermore, ΔH_{pp} becomes smaller and the absorption derivative I becomes larger.

In Figure 6.8.b, the difference in the absorption derivative I for a positive current $+J_c$ and negative current $-J_c$ is shown. A clear resonance structure is visible, which demonstrate that the FMR spectra are significant modified in response to current reversal [58]. This indicates that the magnetization relaxation depends on the current direction. When $J_c > 0$ ($J_c < 0$), the injected spincurrent exerts a spin torque on the magnetization that draws the magnetization towards(away) from the external magnetic field direction and thus modulates the Gilbert damping torque.

6.6 Substrate

In Figure 6.9, ΔH_{pp} and H_r of a Co(3.6)/Cu bilayer grown at room-temperature on substrates of single crystal MgO (cubic, a = 0.421), TiO_2 (tetragonal, a = b = 0.460 nm, c = 0.296) and Al_2O_3 (hexagonal, a = 0.475 nm, c = 1.299) are shown for an in-plane magnetic field ($\theta_H =$

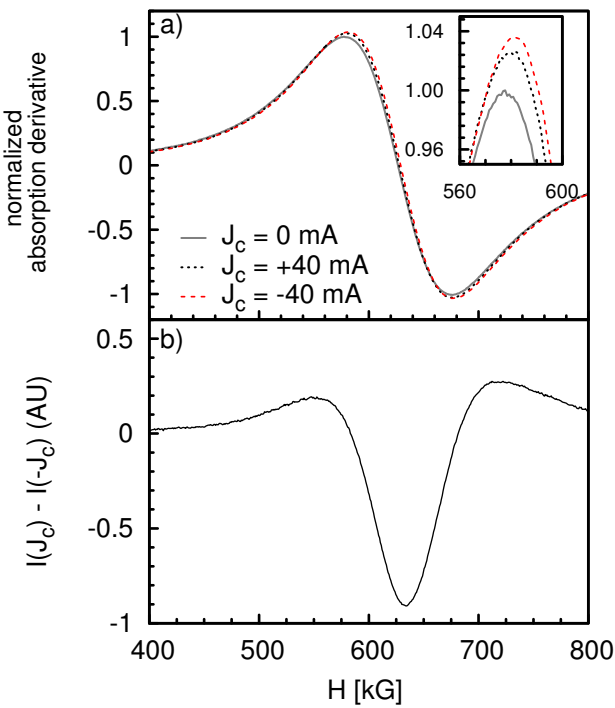

Figure 6.8: a) In-plane ($\theta_H = 90°$) FMR spectra of a SiO_x/Co(5)/Pt bilayer, where the relaxation is manipulated using the SHE. Using the same geometry used to measure V_{ISH}, see Figure 5.8, but now a dc current J_c is sent through the SiO_x/Co(5)/Pt bilayer. The absorption derivative is normalized by dividing the measured values by the maximum absorption derivative when no current is applied. The inset shows magnified views around the peaks of the spectra. b) The difference in the absorption derivative I for a positive current $+J_c$ and negative current $-J_c$ for a applied current of $\pm$40 mA.

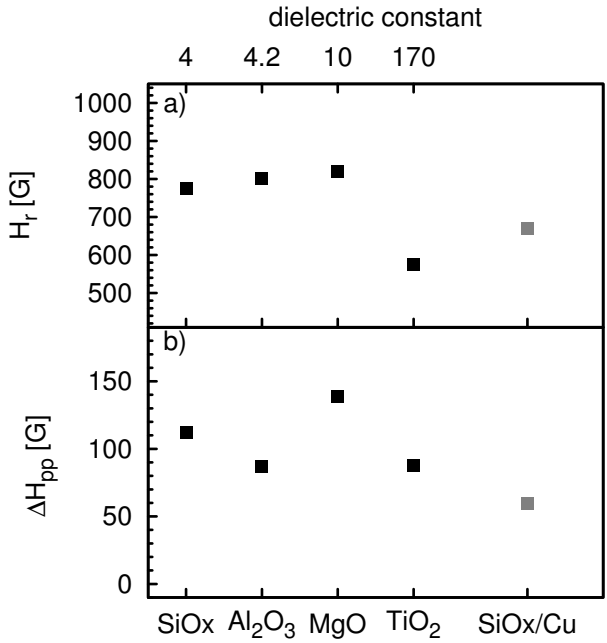

Figure 6.9: The resonance field H_r (a) and the peak-to-peak linewidth $H_{\rm pp}$ (b) of a Co(3.6)/Cu bilayer grown on a single crystal MgO, TiO_2, Al_2O_3 for an in-plane magnetic field ($\theta_H = 90°$). As a reference, also Si with a native oxide layer and a Cu buffer layer are shown.

$90°$). Clearly visible in Figure 6.9.a is that there is a slight variation in H_r for the SiO_x, MgO and Al_2O_3, but H_r of the Co/Cu bilayer grown on TiO_2 and SiO_x/Cu is much smaller.

$\Delta H_{\rm pp}$, as shown in Figure 6.9.b, shows however a different trend. $\Delta H_{\rm pp}$ of the Co/Cu bilayer grown on SiO_x/Cu has the smallest linewidth, the bilayer grown on TiO_2 and Al_2O_3 have almost the same linewidth and $\Delta H_{\rm pp}$ of the Co/Cu bilayer grown on MgO has the largest linewidth.

6.7 Discussion

Summarizing the experimental findings, for very thin Co thicknesses in SiO_x/Co/Cu bilayers, an unexpected large increase in the Gilbert damping and resonance field is observed. In the last three sections, we also observed that the Hall measurements on a SiO_x/Co/Cu bilayer

shows unexpected behavior. Furthermore, various substrates also result in a change of ΔH_{pp} and H_r.

Electric manipulation of the magnetization precession using the SHE

In Figure 6.8.a, the modified spectra of a SiO_x/Co(5)/Pt bilayer are shown. Even with a current of 40 mA, which would for a 2.4×2.4 mm^2 sample result in a current density of approximately 1×10^9 A/m^2, only a change in ΔH_{pp} of approximately 5 % was obtained. A small remark should be made, that the Co layer is 5 nm. When going to thinner Co films, already other mechanisms that influence the magnetization dynamics are more dominant.

Still, the influence of the electric manipulation of the magnetization precession using the SHE does not seem to be the dominant mechanism that results in a large increase of ΔH_{pp} and H_r. Furthermore, the same large increase of ΔH_{pp} and H_r is observed in SiO_x/Co/Cu bilayers. The spin Hall angle of Cu is much smaller than the spin Hall angle of Pt, therefore a spincurrent generated in a Cu layer due to the SHE will be much smaller than a spincurrent generated in a Pt layer due to the SHE. The change in H_r and ΔH_{pp} are than expected to be very small in a SiO_x/Co/Cu bilayer.

Substrate

When growing the Co(2.6)/Cu bilayer on different substrates, a big difference in the in-plane H_r and ΔH_{pp} is visible, as shown in Figure 6.9. These bilayers were grown in the same deposition run, so the sample-to-sample growth variation of the Co(2.6)/Cu bilayer is very small, but no effort was made to optimize the growth to obtain epitaxial layers. However, there are a few differences between the samples. First, the Co/Cu bilayer grows probably slightly different on each substrate, because the lattice constants of each substrate is slightly different. Secondly, the interface between the Co and the substrate is different, resulting in a different interface anisotropy K_s and thus also a different PMA, M_{eff} and H_r. Monso et al. [171, 172] and Yang et al. [173] showed that despite the weak spin-orbit interaction at the interface, a PMA is observed for the substrate/Co interface that is comparable to or even larger than a Co/Pt or Co/Pd interface. H_r in Figure 6.9.b show a slow increase for a SiO_x, Al_2O_3 and MgO substrate, but a dramatic decrease (75 % of the H_r of SiO_x) for the the TiO_2 substrate. The in-plane resonance condition, equation 5.9, indicates that such a large decrease in

H_r would corresponds to a considerable change of either the g-factor or M_{eff}.

However, such a large change in M_{eff} or the g-factor is not likely, which suggest a negative field-like torque, due to the broken inversion symmetry. The very large dielectric constant of TiO_2, which is more than 40 times as large as the dielectric constant of Al_2O_3, might even further increase the size of this field-like torque.

Although H_r of the TiO_2/Co(2.6)/Cu bilayer is much smaller than to the Co(2.6)/Cu bilayer grown on the other substrates, ΔH_{pp} is almost the same as the Al2O_3/Co(2.6)/Cu bilayer as shown in Figure 6.9.a. ΔH_{pp} of the Co(2.6)/Cu bilayer grown on MgO and SiOx are much larger. However, without a full angular dependence analysis, the different contributions to ΔH_{pp} cannot easily be identified.

To conclude, we observe a large increase in the damping, and a change in the resonance field, for thin Co films in asymmetric SiO_x/Co(d)/Cu bilayers. This effect is absent in symmetric Cu/Co/Cu trilayers, and therefore not attributable to spin pumping effects. We suggest that this is due to the presence of spin-orbit torques caused by the broken inversion symmetry of the ferromagnetic heterostructures. We note that the effects are not small, with a field-like torque contribution of about 250 G, and a spin-transfer-like contribution of the order of 100 G.